WING-BODY INTERFERENCE. ON A GENERALIZED LOAD DISTRIBUTION ON THE BODY DUE TO TRIANGULAR WINGS AT SUPERSONIC SPEEDS+

Erik S. Larson
The Aeronautical Research Institute of Sweden
Stockholm, Sweden

Abstract

A generalized load distribution on the body due to interference from triangular wings with supersonic trailing edges and with sufficiently long root-chords is developed by means of an approximate analyses for wing-body combinations without an afterbody at small angles of attack. By an empirical approach the loading on the afterbody has also been predicted with reasonable accuracy and the whole interference load distribution on the body can therefore be condensed into a kind of an approximate similarity law.

The generalized load distribution is compared with a large number of experiments and with the panel method result. The correlation is quite satisfactory.

Symbols

b	wing span
$C_{N(B)} = \frac{N_{(B)}}{q \cdot \frac{\pi D^2}{4}}$	interference normal-force coefficient on the body due to the wing
$C_{m(B)} = \frac{m_{(B)}}{q \cdot \frac{\pi D^2}{4} \cdot c}$	interference pitching-moment coefficient on the body due to the wing
c	root-chord
D	body diameter
h	wing thickness
k(D)	upwash factor
k(τ)	thickness factor
M	Mach number
$N_{(B)}$	normal-force increment on the body due to interference from the wing
$m_{(B)}$	pitching-moment increment on the body due to interference from the wing
p	local pressure
Δp	pressure difference
$\Delta C_p = \frac{\Delta p}{q}$	pressure difference coefficient
q	dynamic pressure
R	body radius
S	interference area
s	half span of the wing
t	time or parameter in load distribution
V	speed
x,y,z	orthogonal coordinates
α	angle of attack
$\beta = \sqrt{M^2-1}$	Prandtl-Glauert factor
ε	half the apex angle
Λ	sweep angle
λ	taper ratio
μ	Mach angle
ρ	density
$\sigma = \frac{c}{\beta D}$	dimensionless chord
θ	polar angle
τ	thickness of the wing
φ	potential function (wing-)
ω	frequence
ξ, η, ζ	dimensionless orthogonal coordinates

Indices

AC	denotes aerodynamic center
ℓ	denotes leading edge
m	denotes mean value
t	denotes trailing edge
tb	denotes trailing edge of the body
trc	denotes trailing edge of the root-chord
∞	denotes free-stream

+ This research has been supported by the Materiel Administration of the Armed Forces, Air Materiel Department, Missiles Directorate, Sweden.

1. Introduction

The ideas and main result of this paper were originally compiled in a preliminary draft[15] of 1961 and only lately it occurred it could be of some interest to make a comparison with experiments[22] at higher Mach numbers and with the result of the panel method[16-20].

Let's therefore take a retrospective glance on the stand of the art up till 1960 concerning wing-body interference.

Theoretical investigations of the supersonic wing-body interference problem seem to have been initiated during the late 1940's in USA (and Italy) by several researchers as Ferrari[1], Lagerstrom and van Dyke[2], Morikawa[3], Nielsen[4] and others. Early studies started in England by Kirkby and Robinson[5]. On the experimental side early contributions were given by Cramer[6,7], Nielsen and Pitts[8] and others. The stand of the art in early 1950's has been given in a survey by Lawrence and Flax[9]. From this it could be judged that the theories aiming at the determination of the interference load distribution on the body were more or less stuck in the mathematical difficulties of obtaining a fast enough convergence of the solution of the quite easily formulated and also well put mathematical problem as such. The restriction to rectangular wings of a certain minimum geometry did also give little hope of getting from the solutions some useful help in a critical project design situation.

In parallel with those contributions to the elucidation of the complete wing-body interference problem by means of linear aerodynamic theory some very striking results were obtained within the theory of slender bodies by Ward[10], Kirkby and Robinson[5], Flax[11] and others. In the form of ratios between partial loads on a wing-body combination an aersenal of handy short-cut methods for early project usage emerged as a possible complement to the more advanced theoretical solutions that sooner or later had to be developed. A great deal of experimental results was needed, however, to check the reliability of the simple ratios. An early control by Cramer[6] on a rectangular wing-body combination at M = 2 gave a surprisingly good correlation for the ratio between the interference normal-force on the body and the total normal force on the wing, for instance.

With the above circumstances as a background some minor investigations in the supersonic region of the wing-body interference field were started in order to collect experiences of our own of the problemacy. The work resulted in experimental and theoretical contributions[12-14], among others.

It was felt as a demanding task to get out from the experiments as much as possible of usable information for project design purposes, let it be the approximative or the empirical way. The load distribution on the body due to the wing being one of the clue items in the wing-body interference problem was thus focused on[12,13]. With a good knowledge of the load distribution important problems within aerodynamic stability and structural design could be evaluated, for instance. If again also the experimental results could be condenced in an analytical form the flexibility of the mentioned short-cut methods would also be gained.

Triggered by reference 1 the idea of culmination or saturation of the interference on the body due to a semi-infinite wing occurred and the experiment[13] was conducted to investigate its realism. Reference 2 gave an inspiration to simplify the estimation of the interference load to just a multiplication of an interference area with a mean pressure coefficient. If the load distribution on the body could be generalized for a spectrum of leading and trailing-edge sweep-angles on unclipped wings a variety of interference problems could be tackled the semi-empirical way.

The present paper is a condenced version of the accompanying engineering report[26].

2. Fundamentals and approximations

2.1 Simplified analyses

The aerodynamic load on a body can be written, external forces being neglected;

$$-\hat{F} = -\left\{ \int_S p\hat{dS} + \int_S \rho\hat{q}(\hat{q}\hat{dS}) \right\} \qquad (1)$$

where S can be a surface whatsoever that surrounds the body, i.e. the body-surface itself. The second r.h. term gives the suction force along the leading-edge and is neglected here. What is left is then:

$$-\hat{F} = -\int p\hat{dS} \qquad (2)$$

where the vectors are $\hat{F} = (X,Y,Z)$ and $\hat{dS} = (dS_x, dS_y, dS_z)$, respectively.

In the following the increment in normal-force, only, on the body due to interference will be treated. It is anticipated that this can be done by means of an equation in analogy with Eq. (2), i.e. the normal-force increment on the body is read, for instance:

$$N_{(B)} = \int_{S_z} \Delta p(x,y)\, dS_z \qquad (3)$$

where $\Delta p = p_u - p_\ell$ is the pressure difference between two antipodal points on the body sureface, $z_u(x_1,y_1)$ and $z_\ell(x_1,y_1)$. S is named the interference-area on the body and S_z is its projection in the x-y-plane.

It is anticipated now that the integral in Eq. (3) can be replaced by a suitable mean pressure difference over a suitable interference-area on the body. The former being proportional to the pressure difference through the wing close to the body-side. A body upwash factor has to be included in order to make the approximation reasonable.

Eq. (3) is thus simplified to:

$$N_{(B)} = \overline{\Delta p} \cdot S_z \qquad (4)$$

After differentiation with respect to x the load distribution on the body is obtained:

$$\frac{d(N_{(B)})}{dx} = \overline{\Delta p} \cdot \frac{dS_z}{dx} \qquad (5)$$

Eq. (5) is now used as a common starting point together with the anticipation of a flow without losses, for estimating the interference load distribution on the body on a number of missile configurations, especially, where the wing is the interference generating component as shown in Fig. 1.

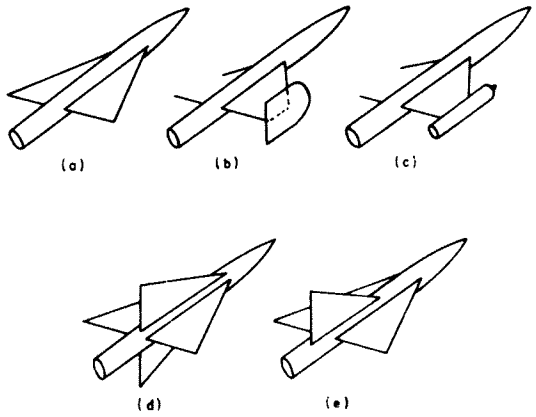

Fig. 1. Some slender wing-body combinations where interference is an important design feature.

The cases a) and c), only, for wings with arbitrary leading-edge sweep-angles will be treated here. The restriction has herewith to be made that the span and the root-chord of the wing shall be, both of them, of a sufficient length to allow saturation of the interference to develop on the body, i.e. the wing must behave itself as if it were semi-infinite. The conditions are necessary for avoiding the disturbances from the wing-tips to spoil the evaluation of the applied approximations leading to Eq. (5).

3. An approximate load distribution on the body due to a semi-infinite wing

3.1 The rising part of the load distribution

Fig. 2 illustrates how the expected saturation in the load distribution on the body due to a semi-infinite wing is reached at a distance x_∞ from the origin. The sharp corner at $x = x_\infty$ does not exist in reality, where a gradual increase of the load distribution towards a maximum can be recognized.

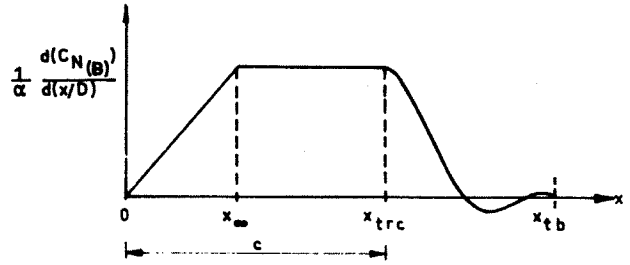

Fig. 2. A schematic interference load distribution on the body.

As a starting point for the derivation of the rise of the load distribution on the body due to interference from a wing with an arbitrary leading-edge contour line it is anticipated that the load increment on the longitudinal body-element $\Delta x'$, cut off by the planes x' and $x' + \Delta x'$ at right angles to the body axis is proportional to the element of the wing area that is cut out by those planes from a wing that is transformed with respect to the freestream Mach number.

By means of the co-ordinate system in Fig. 3 the rate of increase in the x-direction of the area of the transformed right wing-panel can be determined when the leading-edge contour is given by the equation $y = f_1(x)$.

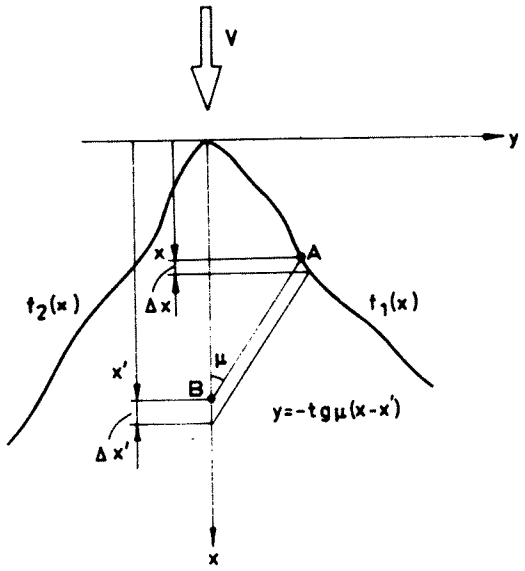

Fig. 3. The transformation of the planform of a wing.

At x is obtained if $Y_1(x)$ is the area from $x = 0$ to x of the given (physical) wing,

$$\frac{dY_1}{dx} = f_1(x)$$

At x' is obtained:

$$\frac{dY_1}{dx'} = \frac{dY_1}{dx} \cdot \frac{dx}{dx'} = f_1(x)\,\frac{dx}{dx'} \qquad (6)$$

The cross-over point of the line AB and the leading edge, $f_1(x)$, is given by:

$$f_1(x) = -\tan\mu(x-x'), \quad \text{i.e.}$$

$$x = \frac{x'\tan\mu - f_1(x)}{\tan\mu} \qquad (7)$$

The derivative of Eq. (7) with respect to x' gives:

$$\frac{dx}{dx'} = \frac{1}{1 + \frac{f_1'(x)}{\tan\mu}} \qquad (8)$$

Inserting Eq. (8) in Eq. (6) gives:

$$\frac{dY_1}{dx'} = \frac{f_1(x)}{1+\beta f_1'(x)}\,, \qquad \beta = \frac{1}{\tan\mu} \tag{9}$$

For the left wing-panel a similar expression is obtained and thus the mean rate of increase of area is:

$$2\frac{dY}{dx'} = \frac{dY_1}{dx'} + \frac{dY_2}{dx'} = \frac{f_1(x)}{1+\beta f_1'(x)} + \frac{f_2(x)}{1+\beta f_2'(x)} \tag{10}$$

If specializing to a symmetric wing it is obtained:

$$\frac{dY}{dx'} = \frac{f(x)}{1+\beta f'(x)} \tag{11}$$

Eq. (11) can be looked upon as the ability of the given (physical) wing to shadow a body placed in the trace between the plane of the wing and the plane of symmetry. The incremental load distribution on the body due to the interference from the physical wing will be, approximately, proportional to Eq. (11). The factors of proportionality are, on the one hand, the mean pressure difference, $\overline{\Delta p_v}$, between lower and upper side of the wing in the neighbourhood of the body, and the upwash characteristics of the body, $k(D)$, on the other.

Denoting the increments of the pressure and normal-force differences in the section x' on the body due to presence of the wing by $\Delta p_{(B)}$ and $N_{(B)}$, respectively, it is obtained:

$$\frac{d(N_{(B)})}{dx'} = 2\int_0^{D/2} \Delta p_{(B)}\,dy \cong \overline{\Delta p_v}\cdot k(D)\cdot\frac{f(x)}{1+\beta f'(x)} \tag{12}$$

According to wing-theory the pressure difference through the wing-surface can be denoted:

$$\Delta p_v = \rho V\,\frac{\gamma(x,y)}{\beta} \tag{13}$$

where $\gamma(x,y)$ is a distribution of singularities in incompressible flow. The strength of the vortex-distribution at the point (x,y) shall be such, that the kinematic boundary condition is fulfilled at that very point on the here treated nearly two-dimensional wing-element.

On a plane wing near the body-side it is anticipated now that the simple boundary condition still holds, as if the body was not there at all, i.e.

$$V\alpha \cong \frac{1}{2}\gamma(x,y) \tag{14}$$

where V and α are free-stream velocity and angle of attack, respectively.

Inserting Eq. (14) in Eq. (13) and Eq. (12) it is obtained when the prime sign on x and the $\sim$ -sign are discarded,

$$\frac{d(N_{(B)})}{dx} = 2\cdot k(D)\frac{\rho V^2\alpha}{\beta}\,\frac{f(x)}{1+\beta f'(x)} \tag{15}$$

Specializing Eq. (15) to a wing with a linear leading-edge of the form,

$$y = f(x) = x\,\tan\varepsilon\,, \qquad f'(x) = \tan\varepsilon\,,$$

where ε is the half of the apex-angle, it is obtained from Eq. (15):

$$\frac{1}{\alpha}\,\frac{d(C_{N(B)})}{d\xi} = k(D)\cdot\frac{16}{\pi}\cdot\frac{\beta\tan\varepsilon}{1+\beta\tan\varepsilon}\cdot\xi \tag{16}$$

when the normal-force is referred to the area of the body cross-section (that here is circular) and a dimensionless length, $\xi = x/\beta D$, is introduced.

According to Eq. (16) the load distribution increases linearly with ξ. This, however, can only go on up to a certain $\xi = \xi_\infty$, where, depending on the combination of ε and M, the saturated (maximal) interference is reached.

For a straight leading-edge wing, $\varepsilon = \pi/2$, it is received for $\xi = 1$ when the upwash is neglected $(k(D) = 1)$,

$$\frac{1}{\alpha}\,\frac{d(C_{N(B)})}{d\xi} = \frac{16}{\pi} \quad \text{at} \quad \xi = 1\,,$$

which is Ackeret's result referred to the area of the body cross-section.

For $\xi > 1$ it is now anticipated that the load distribution is a constant for a semi-infinite wing.

Comparing Eq. (16) with Eq. (5) it is seen that they are equivalent and that a dimensionless expression of $\overline{\Delta p}$ now has been obtained which can be utilized on wings with arbitrary leading-edge sweep angles. The $\overline{\Delta p}$ in Eqs. (5) and (16) can also be derived by means of slender body-theory as shown in reference 26.

3.2 An approximation of the interference-area on the body

When deriving Eq. (16) nothing was said to regulate the form of the interference-area and therefore it increases linearly with ξ. This is not in accord with reality. From flow-pictures it had been noticed that the area on the body influenced by the wing had boundaries of parabola-like contours, that did not start at the leading-edge of the root-chord, but rather at a certain distance in front of this point, as a probable concequence of the thickness of the wing. These observations were used for an empirical estimation of an interference-area that could cooperate in a satisfactory way with the approximate mean pressure difference. The artificial point $\xi = \xi_\infty$ was chosen to be at $\xi = \xi_\infty = \pi/2$.

With the definitions in Fig. 4 the equation of the actual parabola is,

$$\zeta'^2 = p(\xi + \tau) \tag{17}$$

where τ is the wing thickness, for instance.

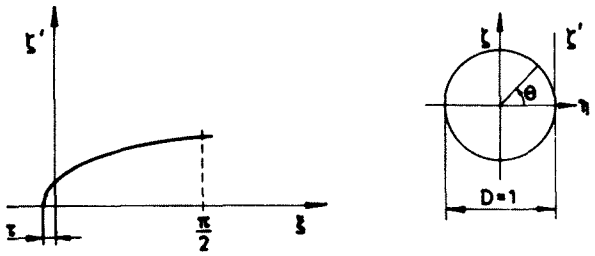

Fig. 4. The estimation of the interference-area on the body by means of a parabola.

When the curve is folded around the surface of the cylinder the growth in ξ-direction of the projection in the ξ-η-plane of the interference-area is therefore approximated to,

$$\frac{d\Sigma_\zeta}{d\xi} = 1 - \cos\left(\frac{\pi}{2} \sqrt{\frac{\xi+\tau}{\pi/2+\tau}} \right) \qquad (18)$$

Eq. (18) is a dimensionless counterpart to dS_z/dx in Eq. (5).

When the r.h. part of Eq. (18) is inserted in Eq. (16) to replace ξ, it is obtained,

$$\frac{1}{\alpha} \frac{d(C_{N(B)})}{d\xi} = k(D) \frac{16}{\pi} \frac{\beta \tan\varepsilon}{1+\beta\tan\varepsilon} \left(1 - \cos\left(\frac{\pi}{2} \sqrt{\frac{\xi+\tau}{\pi/2+\tau}} \right) \right) \qquad (19)$$

Eq. (19) now describes the growth of the load distribution on the body in the domain $0 \leq \xi \leq \pi/2$ when two equal wing-halves are present. In case of one wing-panel only (wing-tip-body) the Eq. (19) is, after dividing by a factor of 2, applied in the domain $0 \leq \xi \leq \pi$.

An approximation of a suitable upwash factor $k(D)$ will be given in the next section.

When inspecting the experiments and the panel method results at $M = 4$ and 7.15 it became evident, that the wing thickness had a quite strong influence on the whole load distribution and that this to a large extent could be adjusted for by an explicit factor, at the side of the thickness influenced term in Eq. (19), that seems to fill its purpose quite satisfactorily for thin wings at $M < 3$. At the higher Mach numbers, therefore, a wing thickness factor of the form

$$k(\tau) = 1 + M \cdot (h/c)_m = 1 + \tau \qquad (20)$$

with $(h/c)_m$ being the mean thickness of the wing, is inserted as a multiplying factor in Eq. (19).

3.3 A schematic upwash factor, k(D)

From the interference load distribution on the body of a family of wing-body combinations with straight leading-edge wings of different span at $M = 1.59$, it is recognized, that a half-span of about $y = 8R$ is needed for saturation in the interference load distribution on the body to be reached. Intuitively a much smaller span would have been expected to suffice. However, the thus received "fictive span $\bar{y}$" for saturation to develop for $\Lambda_\ell = 0$ is now anticipated as a norm even for swept wings and also for Mach numbers $M \neq 1.59$. The dimensionless fictive span for arbitrary sweep angles is thus obtained as a function of β, $\bar{y}/R$ and Λ_ℓ, and a kind of an upwash factor can be formed, namely,

$$k(D) = 1 + (R/y) \ , \qquad (21a)$$

where

$$(R/y) = \frac{\beta + \tan\Lambda_\ell}{\beta(\bar{y}/R) + \tan\Lambda_\ell} \qquad (21b)$$

and $\bar{y}/R = 8$.

When Eq. (21) is used on wing-body combinations A to D with leading-edge sweep-angles from $\Lambda_\ell = 0$ to 80° the upwash factor $k(D)$ is changing with the Mach number as seen in Table 1.

Config	Λ_ℓ [grad]	M = 1.59 β = 1.235		M = 2.98 β = 2.81		M = 4 β = 3.88		M = 7.15 β = 7.07	
		(y/R)	k(D)	(y/R	k(D)	(y/R)	k(D)	(y/R	k(D)
A	0	8	1.125	8	1.125	8	1.125	8	1.125
B	45	4.85	1.206	6.16	1.162	6.35	1.157	7.02	1.142
C	63.4	3.68	1.272	5.1	1.196	5.61	1.178	6.47	1.155
D	80	2.26	1.443	3.28	1.305	3.84	1.261	4.88	1.204

Table 1. The semi-empirical factor, k(D).

Except for straight leading-edge wings, $k(D)$ decreases for increasing Mach number. The empirical upwash factor is analogous with the Ward factor:

$$\frac{L_{w(B)}}{L_w} = 1 + R/s_m$$

and the Nielsen factor:

$$K_w = f(s_m/R) \ ,$$

respectively. Those factors are, however, tied up with the maximum span of the wing, s_m, and do not vary with the Mach number.

The primitive upwash factor, Eq. (21), has got the merits to serve its present purpose as a simple multiplicative factor that is a kind of mean value between a theoretically derived upwash factor and another factor expressing the gasdynamic losses along the wing-body juncture.

3.4 An empirical load distribution on the afterbody

From experiment it was known that the interference load distribution changes its sign on the afterbody at a certain distance behind the trailing-edge of the root-chord as sketched in Fig. 2. This follows from the compressions and the expansions of the flow across the trailing-edge of the wing. Instead of trying to describe this very complicated flow situation theoretically an empirical simulation of the decreasing branch of the interference load distribution itself was looked for. Thus a suitable analytical expression was found that could be forced through adjustment of some constants

to correlate in a satisfactory way the experiments at M = 1.59 and 2.98 (the only available), and that at the same time was easily integrable (to give the afterbody load).

The chosen equation is:

$$z = z_{trc}(1-\bar{\xi})\exp(-\frac{t}{2}\bar{\xi}^2) \qquad (22)$$

with

$$\bar{\xi} = \frac{\xi - \xi_{trc}}{\xi_o'} \geq 0 \quad ,$$

where z_{trc} shall be replaced by the load value due to the interference on the body at the trailing-edge of the root-chord ($x = x_{trc}$) and

$$t = \frac{0.55 + \beta + \cos\Lambda_\ell}{4} \qquad (23)$$

and

$$\xi_o' = \sqrt[3]{\xi_o} \qquad (24)$$

are estimated empirically after ξ_o having been determined by means of the wing planform characteristics and the sine-theorem:

$$\xi_o = \frac{\overline{CD}}{\beta D} = \frac{c}{\beta D}\frac{\cos\Lambda_\ell \cos(\Lambda_t+\mu)}{\sin(\Lambda_\ell+\Lambda_t)\sin\mu} \qquad (25)$$

for

$$\Lambda_\ell + \Lambda_t \neq 0 \ .$$

3.5 The approximate load distribution compared with experiment and with theory

The approximate load distribution on the body due to the interference from a triangular wing at supersonic speeds can now be given in an analytical form by combining the results of the previous sections. It reads:

$$\frac{1}{\alpha}\frac{d(C_{N(B)})}{d\xi} = k(\tau)\ k(D)\ \frac{16}{\pi}\frac{\beta\tan\varepsilon}{1+\beta\tan\varepsilon} \cdot$$

$$\cdot \begin{cases} (1-\cos\frac{\pi}{2}\sqrt{\frac{\xi+\tau'}{\pi/2+\tau}}) \ , & 0 \leq \xi \leq \frac{\pi}{2} \\ (1), & \frac{\pi}{2} \leq \xi \leq \xi_{trc} \\ (1-\bar{\xi})\exp(-\frac{t}{2}\bar{\xi}^2), & \bar{\xi} \geq 0 \end{cases} \qquad (^{26}_{a,b,c})$$

where

$$\xi = \frac{x}{\beta D} \ , \text{ and}$$

$\bar{\xi}$ and t are defined in Eqs. (22) through (25),

and

$$k(\tau) = 1 + M(h/c)_m \qquad [(20)]$$

and

$$k(D) = 1 + \frac{\beta + \cot\varepsilon}{\beta(\bar{y}/R) + \cot\varepsilon} \ , \ (\bar{y}/R = 8) \qquad [(21)]$$

The approximate load distribution is compared in Fig. 5 through 8 with experiments from references 12, 13 and 22 in the supersonic speed interval M = 1.47 to 7.15. In the same diagrams the numerical results obtained by the panel method[16-20], received from references 23 and 24, have been inserted.

The wing-body combinations in the mentioned references consist of ogive-noses and cylinder bodies with triangular wings. The leading-edge sweep-angles are ranging from $\Lambda_\ell = 0$ to 80^o and the wings are fixed to the body in the horizontal plane through the body symmetry axis. On the configurations studied at the lower Mach numbers the wings are flat, thin plates with rounded off leading-edges and straight cut off trailing edges. On the models examined at M = 4 and 7.15 the wing section at right angle to the leading-edge is a wedge with a rounded off profile nose, that has a constant thickness along the leading-edge. The trailing-edge is here also straight cut off. All the trailing-edges, but on one wing (M = 1.47[12]), are swept forward $\Lambda_t = 45^o$. The main geometric data of the test models are collected in Table 2.

Mach number M	Model code	L.E. sweep angle Λ_ℓ[°]	T.E. sweep angle Λ_t[°]	Span ratio b/D	Taper ratio λ	Root chord ratio c/D
1.47	C6.9	63.4	0	6.9	0.16	7.02
1.59	A12	0	45	12	0	5.5
	B7.5	45	45	7.5	0	6.5
	C3.5	63.4	45	3.5	0.423	6.5
	D4	80	45	4	0	10
	D2.95	80	45	2.95	0	6.5
2.98	A5	0	70	5	0	5.5
	B5.23	45	64.6	5.23	0	6.5
	C5.33	63.4	45	5.33	0	6.5
	D2.95	80	45	2.95	0	6.5
4	C4.34	63.4	45	4.34	0	5
	D2.5	80	45	2.5	0	5
7.15	C4.34	63.4	45	4.34	0	5
	D2.5	80	45	2.5	0	5

Table 2. The main geometrical data of the wing body test models.

In the following the wing thickness has been neglected for M < 3, except in one case for illustration, wing A at M = 1.59. At M = 4 and 7.15 the influence of the thickness will be inspected more in detail.

The experimental peak values in Fig. 5a are probably conservative because of wing bending due to the large wing-span and the small wing-thickness leading to a marked dihedral during the tunnel test. The test points in the same area in Figs. 6a and 7 also probably are too low, because the wings here are too small (too short a root-chord) to give maximum interference on the body at these Mach numbers.

In Fig. 5a Ferrari's classical result[1] generalized by Rae[25] to all straight leading-edge wings with infinite span has been inserted. The load distribution has been obtained with the first step of iteration of Ferrari's solution. Regardless the load distribution on the afterbody, which is erroneously described, it is

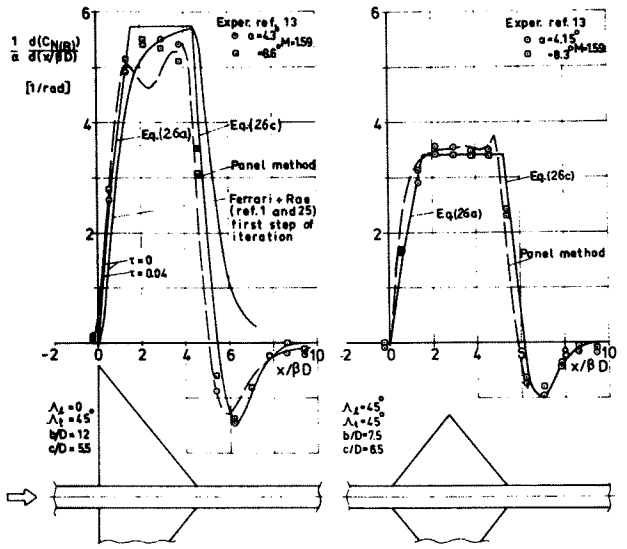

a) The model A12 b) The model B7.5

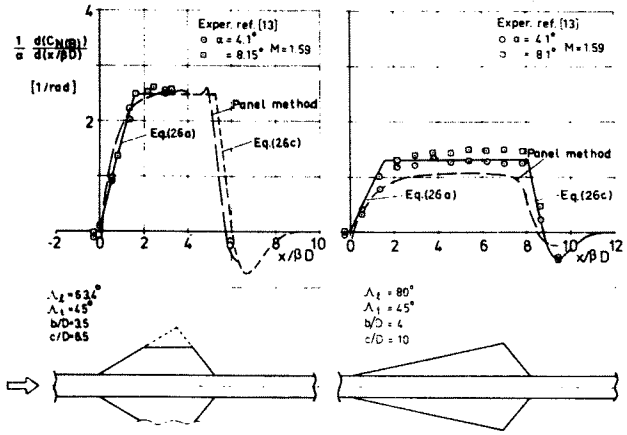

c) The model C3.5 d) The model D4

Fig. 5. The interference load distribution on the body due to triangular wings at M = 1.59. Comparison between different theories and experiment.

evident that the qualitative trend of the experiment is well predicted by Ferrari's theory.

The panel method result in Fig. 5a has got in this particular case a depression in the region for the maximum load distribution, an error, that probably can be removed, if another panel subdivision on the wing and the body is chosen. The increasing branch as well as the decreasing one of the load distribution are in good accord with the experiments. The negative peak value and negative area of the afterbody load distribution are, however, smaller than the corresponding experimentally obtained values.

From Fig. 5a it is seen that the approximate interference load distribution on the body is in good accord with experiment and with Ferrari's theory (the rising part of it) and that the results, as a whole, are well supported by the result of the panel method. A minor shift to the left of whole the approximate load distribution on the afterbody would improve the correlation with experiment, however.

In Fig. 5b through 5d the comparison between the approximate load distribution, experiment and the panel method is continued at M = 1.59 on more and more slender combinations. It can be noticed that as a whole the correlation between the results of the three methods are good though certain typcial differences exist. The panel method gives a more convex increasing branch of the load distribution and probably underestimate the negative part of it in comparison with the experiments. The sharp corner at $\xi = \pi/2$ in the approximate distribution has of course no physical relevance.

For the most slender combination ($\Lambda_\ell = 80^o$) there is a marked difference between the results of the approximate theory and the panel method. The reason for this probably is two-fold. In the first place, the predicted k(D)-factor may be too high by a not intended inclusion of a certain quantity that could be labelled a non-linear contribution, and on the other, the panel method gives a slight underprediction of the linear interference load distribution on the body. The real linear interference load distribution therefore ought to be found somewhere in-between the two results, below and probably quite near the experimental points at $\alpha = 4^o$ on the positive branches of the load distribution.

In Fig. 6a to 6c comparison is made at M = 2.98. In Fig. 6a the increasing part of the load distribution, only, can be strictly compared with the experiment because the physical wing has got a smaller span than the one used at the panel method computation. The panel method result correlates very well with experiment in this part of the load distribution. The approximate theory first undershoot the experiment and then overestimate the maximum load. The latter overshoot could be caused by a not accurate upwash factor k(D) . The decreasing branch of the experimental distribution is, however, quite well predicted by the approximate theory. The decreasing branch for the larger wing, determined by the panel method and by the approximate theory and shown in the diagram turns out to be practically alike.

In Figs 6b and 6c again the more convex shape of the panel method result for the increasing branch of the distribution gives a better correlation with the experiments in this region than the more flat shape received by the approximate theory. The latter method, on the other hand, predicts the negative part of the distribution in slightly better accord with the experiments. For the most slender combination ($\Lambda_\ell = 80^o$) the approximate theory, as it does at M = 1.59, overpredicts the maximum value of the load distribution. Here again the reason for this is that the upwash factor k(D) probably is too high.

In Fig. 6d the approximate theory and experiments, only, are compared at M = 1.47. The

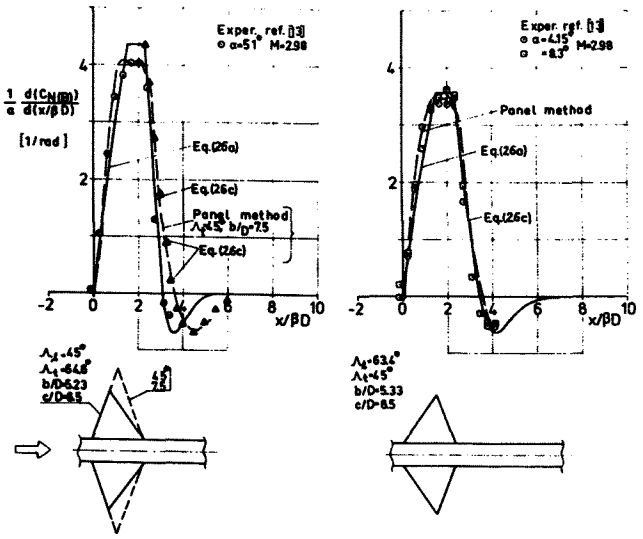

a) The model B5.23 b) The model C5.33

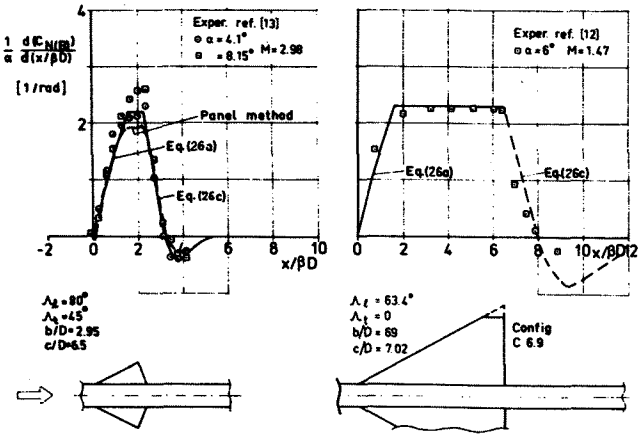

c) The model D2.95 d) The model C6.9

Fig. 6. The interference load distribution on the body due to triangular wings at M= 2.98 and 1.47. Comparison between different theories and experiment.

wing has clipped tips and therefore the two load distributions on the afterbody are not comparable. It might be that the upwash factor, k(D), here is slightly too high, because at $\alpha = 6^{o}$ a certain amount of nonlinearity in the overall lift is to be expected on a quite slender configuration like this one.

In Fig. 7 the interference load distribution on the body at M = 4 and 7.15, obtained by experiment and by the approximate theory, are shown. The latter distribution, however, is determined for combinations with anticipated wings, that are just large enough to cause the interference to reach its maximum value. The supposed enlargement of the respective wings for this to occur is shown on the corresponding configuration sketches. The theoretical distribu-

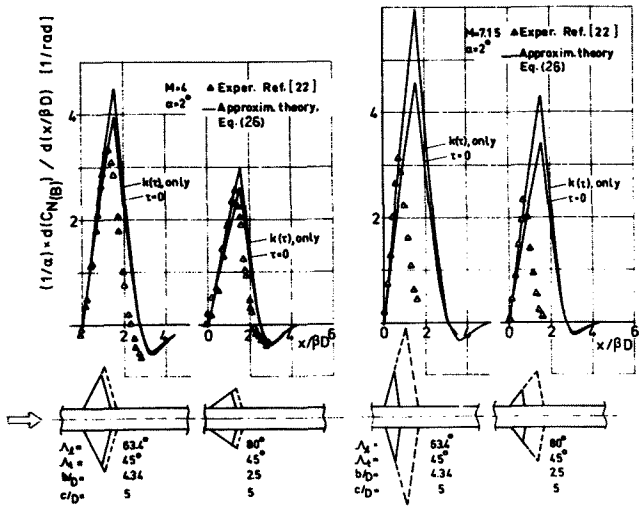

The models C4.34 and D2.5 at

a) M = 4 b) M = 7.15

Fig. 7. The interference load distribution on the body due to triangular wings at M = 4 and 7.15. Comparison between experiment and approximate theory for enlarged wings.

tions are determined with and without use of the explicit thickness factor. The first part, only, of the increasing branch of the load distribution can be compared with the experiments and it is evident that the explicit thickness factor must be applied in order to obtain correlation with the experiments. Whether or not the high peak value at M = 7.15 is physically relevant is hard to judge about. In order to control this experimentally a test model with a root-chord of the wing not shorter than about 12D must be used. Theoretically a check could be obtained by the panel method.

In Figs. 8a to 8c the experiments in the above diagrams are compared with the results of the panel method and the approximate theory when the afterbody load distribution obtained by the latter method has been reduced in proportion to the ratio between the peak values obtained with the actual wings and with the enlarged wings in the previous Figs. 7a and 7b. This evidently gives a slight deterioration in the correlation with experiments for the negative part of the distribution as can be seen when comparing with Fig. 7a. In order to avoid this it could eventually be recommended to just move the full, unscaled afterbody load distribution to the left, and parallel with itself, till it passes through the peak value of the distribution.

From Fig. 8a it can be seen that the thickness contributions in the load distributions are practically of the same magnitude when determined by the panel method and by the approximate theory. The former theory, however, overestimates the interference load more than the latter when compared with the experiment at $\alpha = 2^{o}$. One typical characteristic for the panel method result is, that the decreasing branch of the load distribution in Figs. 8a and 8b goes approximately paral-

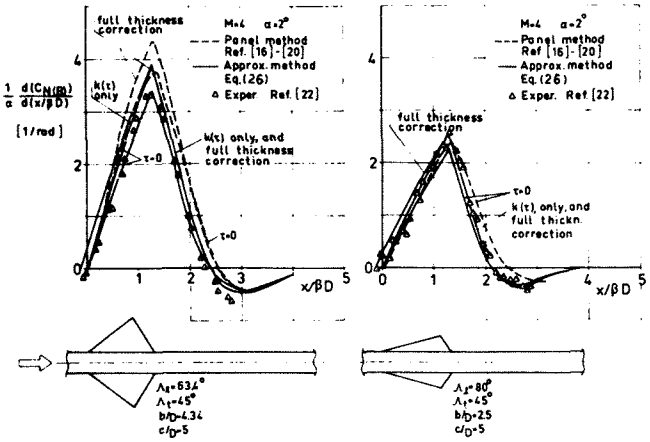

a) The models C4.34 and D2.5 at M = 4

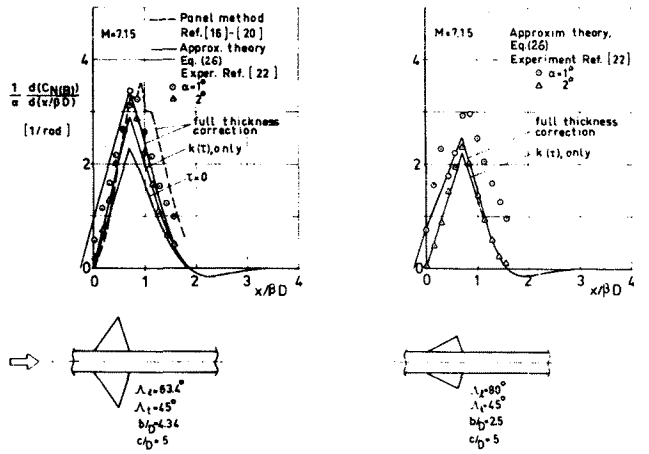

b) The models C4.34 and D2.5 at M = 7.15

Fig. 8. The interference load distribution on the body due to triangular wings at M = 4 and 7.15. Comparison between approximate theory, experiment and panel method.

lel with and to the right of the other two results shown in the diagrams. This probably must be so because the linear theory can not correct for the gasdynamic losses in the wingbody juncture, for instance, and elsewhere on the configuration. The results in Fig. 8c at M = 7.15 seem to support this a great deal by showing a better correlation with experiment at $\alpha = 1^{o}$ than at $\alpha = 2^{o}$. The approximate theory underpredicts the experimental result probably because the upwash factor, k(D), is here too small.

Inclusion of the implicit thickness term leads to an overestimation of the increasing branch of the load distribution for the larger wing-body combination at both Mach numbers compared with experiment as seen from Figs. 8a and 8c. For the slender combination, however, an improvement can be noticed, Figs. 8b and 8d.

4. On a generalized interference load distribution on the body

4.1 The generalized load distribution

When the common factor in the right hand members of Eq. (26) is moved to the left hand side a generalized load distribution is obtained, that depends on a parameter, t, in the afterbody distribution. The load distribution is integrable and the normal-force and pitching moment increments due to interference can thus be obtained in closed form[26] for all triangular wings that are large enough to cause saturation in the interference. When the triangular wing is deformed by clipping the wing tips the load distribution will also be deformed and can not for appreciable croppings be determined by Eq. (26). An extention of the approximate theory to incorporate even such wing planforms is probably possible, however.

In Figs. 9 and 10 the generalized load distribution is compared with experiments. To make easy the comparison all the test points on the afterbody has been moved in order to make the afterbody load distribution start at the same point, $\xi_{trc} = 5.0$, irrespective of the dimensionless root-chord being shorter or longer than that very length.

In Fig. 9 the experiments[12,13] in the Mach number interval M = 1.47 to 2.98 are collected for a comparison with the generalized load distribution. In this case the thickness of the wing has been neglected, i.e. $\tau = 0$ and $k(\tau) = 1$, because the wings are thin.

As could be expected from the previous comparisons in Figs. 5 to 8 the correlation is good enough to support the assumption of the existence of an approximate, generalized interference load distribution on the body at supersonic speeds. With an exception for the most slender combination ($\Lambda_\ell = 80^{o}$) at M = 1.59, for which two to three test points at the fore part on the body fall markedly under the generalized distribution, the majority of test points merges around the curves of the generalized distribution in a quite convincing manner.

An inclusion of the here neglected thickness terms would give a minor improvement of the correlation up till the trailing-edge of the root-chord and would cause at the same time a slight deterioration on the decreasing branch on the afterbody.

In Fig. 10 the experiments[22] at M = 4 and 7.15 are compared with the generalized load distribution. Now the thickness factor $k(\tau)$ has been used, but the implicit thickness terms are neglected.

The test points correlate very well with the rising branch of the generalized distribution. One has, however, to realize that the compression of the scale on the horizontal axes increases strongly with increasing Mach number. Inclusion of the neglected implicit thickness terms would move the starting point of the generalized distribution a minor distance to the left

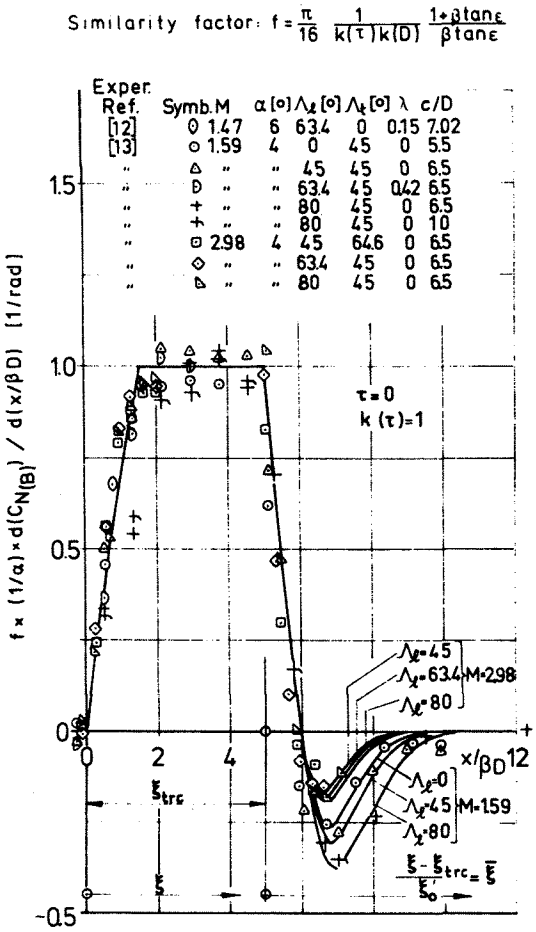

Fig. 9. The generalized load distribution on the body due to interference from triangular wings. Correlation between approximate theory and experiment at M = 1.47 to 2.98.

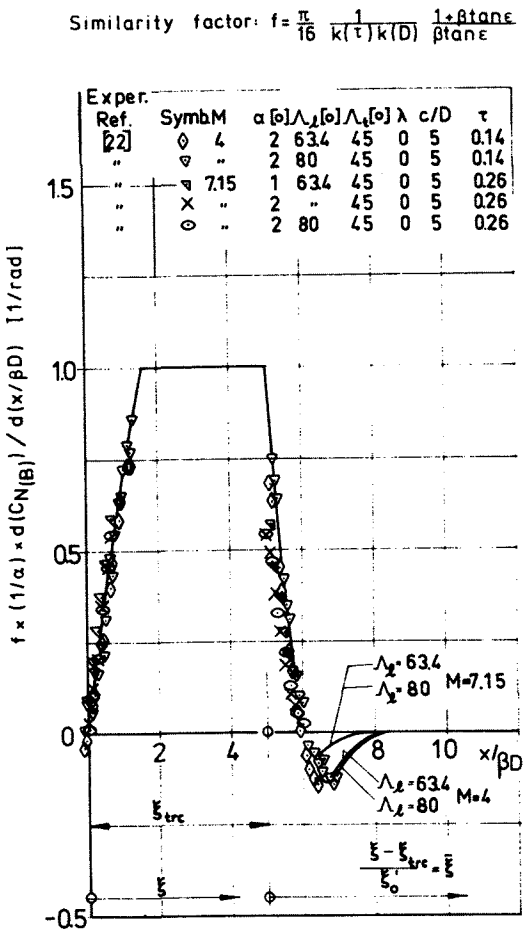

Fig. 10. The generalized load distribution on the body due to triangular wings. Correlation between approximate theory and experiment at M = 4 and 7.15.

of the origin and improve the correlation with the test points at $\alpha = 1^{\circ}$ at M = 7.15, as has already been shown in Fig. 8. At the same time, however, the correlation with experiments at $\alpha = 2^{\circ}$ will be deteriorated.

On the afterbody the correlation at M = 7.15 is less good. The discrepancy could here be referred to the fact, that the wing chords on the triangular wings are too short for saturation in the interference on the body to be reached, and therefore no full afterbody load distribution can be expected. At M = 4 the correlation is quite good because the wings are nearly as large as the necessary minimum for a full afterbody load distribution to occur.

Accepting the last explanation as correct to principle the generalized load distribution on the body in its present simple shape obviously can be discerned up to a Mach number as high as at least seven.

5. The transform of the generalized load distribution

The approximate generalized distribution that has been derived probably belongs to a more common class of similarities realming the compressible flow and which already has been partly disclosed by the not yet fully adjusted similarity laws.

The coordinate system in which the present approximate similarity law is formulated appears in the following way, when a load distribution is given in an orthogonal coordinate system (physical coordinates), $K_3=(x_1, x_2, x_3)$, where $x_1 = x/D$, $x_2 = y/D$, and $x_3 = (1/\alpha)(dC_{N(B)}/dx_1)$.

By means of a linear transformation the coordinate system is changed into a new one in accordance with

$$\bar{y} = T\bar{x}, \quad \text{where} \quad T = \begin{pmatrix} 1/\beta & 0 & 0 \\ 0 & 1 & 0 \\ 0 & 0 & \hat{\beta} \end{pmatrix} \quad \text{and} \quad \bar{x} = \begin{pmatrix} x_1 \\ x_2 \\ x_3 \end{pmatrix}$$

In Fig. 11 some wing series are sketched that give in the transformed system equal pressure and load distributions on the body, and the pressure and load distributions on the wings themselves ought to be equal in this very space.

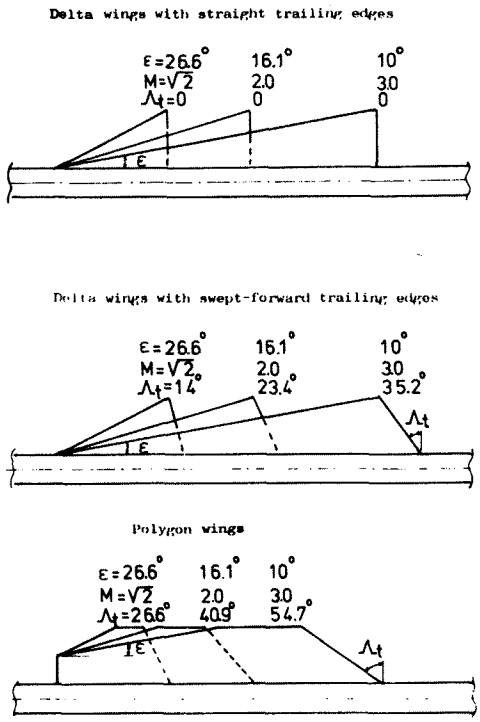

Fig. 11. Some examples of wing-families that are supposed to give in the transformed space the same pressure and load distributions on the body.

Concluding remarks

The simplified aerodynamic assumptions made at the derivation of the generalized interference load distribution on the body have facilitated a great deal the obtainment of a closed form solution that is, however, restricted to triangular wings with supersonic trailing edges and to wings of a certain minimum size. When applied within the limits of definition the interference load distribution shows good correlation with experiments and with the results of the panel method.

The analytical form gives to the result a wanted flexibility that increases the usability. Improvements are welcomed, however, as to the schematic upwash factor, for example, that in this application is used as a resulting upwash factor, combining the real body upwash and the gasdynamic losses in the wing-body juncture. The prediction of the wing-thickness influence and the afterbody load distribution at high Mach numbers probably also can be refined by some quite simple means.

It is probably possible to extend the similarity law to incorporate all possible wing planforms, if suitable experiments and theoretical means are exploited in combination.

The present approximate, generalized load distribution, and still more a refined one valid for arbitrary wing planforms, will hopefully, find a place beside existing short-cut methods as a handy tool in early project work situations and can already be used as an element in existing computerized aircraft and missile project manuals, that in a way are built on fundamental and simplified aerodynamic know-how.

References

1. Ferrari, C
   Interference between wing and body at supersonic speeds. - Theory and numerical application.
   JAS, June 1948.

2. Lagerstrom, P A
   van Dyke, M D
   General considerations about planar and non-planar lifting systems.
   Douglas Aircraft Co. Rept. SM-13432, June 1949.

3. Morikawa, G K
   The wing-body problem for linearized supersonic flow.
   Calif. Inst. of Tech., Doctoral Thesis, 1949.

4. Nielsen, J N
   Supersonic wing-body interference.
   Calif. Inst. of Tech., Doctoral Thesis, 1951.

5. Kirkby, S
   Robinson, A
   Wing-body interference at supersonic speeds.
   College of Aeronautics, Cranfield, Rept. 7, April 1947.

6. Cramer, R H
   Interference between wing and body at supersonic speeds. - Theoretical and experimental determination of pressures on the body.
   JAS, Sept. 1951.

7. Cramer, R H
   Interference between wing and body at supersonic speeds. Part V: Phase one wind tunnel tests correlated with linear theory.
   Cornell Aeronaut. Lab., Bumblebee Rept. CAL/CM-597, December 1950.

8. Nielsen, J N
   Pitts, W C
   Wing-body interference at supersonic speeds with an application to combinations with rectangular wings.
   NACA Tech. Note 2677, 1952.

9. Lawrence, H R
   Flax, A H
   Wing-body interference at subsonic and supersonic speeds. - Survey and new developments.
   JAS, May 1954.

10. Ward, G N

Supersonic flow past slender pointed bodies.
Quart. J. Mech. and Appl. Math., Vol II, Part 1, No. 3, 1949.

11. Flax, A H

Integral relations in the linearized theory of wing-body interference.
J. Aeronaut. Sci. 20, 483-490 (1953).

12. Magnusson, L

Flygtekniska uppsatser. -
Tillägnade Professor Sten Luthander på hans 50-årsdag den 8 december 1955.

13. Larson, E

Bestämning av vinginterferensens belastningsfördelning på cylindrisk kropp vid M = 1.59 och 2.98.
KTH AERO RAPPORT FL 218 (1961).

14. Landahl, M
Drougge, G
Beane, B J

Theoretical and experimental investigation of second-order supersonic wing-body interference.
J. Aeronaut. Sci., Vol. 27, No. 9 (Sept. 1960).

15. Larson, E

Approximativ likformighetslag för maximala interferensen på kroppen vid överljudfart.
KTH AERO TA 267, Tekniskt besked nr 1, 1960.

16. Woodward, F A
Tinoco, E N
Larsen, J W

Analysis and design of supersonic wing-body combinations, including flow properties in the near field. Part I - Theory and application.
NASA CR-73106 (1967).

17. La Rowe, E
Love, J E

Analysis and design of supersonic wing-body combinations, including flow properties in the near field. Part II - Digital computer program description.
NASA CR-73107 (1967).

18. Woodward, F A

Analysis and design of wing-body combinations at subsonic and supersonic speeds.
J. Aircraft Vol. 5, No. 6 (1968).

19. Carmichael, R L

A computer program for the estimation of the aerodynamics of wing-body combination.
(Short working paper obtained together with the computer program from NASA-AMES 1970.)

20. Gustavsson, S A L

A computer program for the prediction of aerodynamic characteristics of wing-body-tail combinations at subsonic and supersonic speeds.
FFA AU-635, Part 2, 1972.

21. Jones, R T

Properties of low-aspect-ratio pointed wings at speeds below and above the speed of sound.
NACA Rept 835, 1946.

22. Larson, E

Pressure distribution measurements on an axisymmetric body with and without delta wings at Mach numbers 4 and 7.
(Presented at EUROMECH 20 Meeting, Cambridge, England, July 30-31, 1970.)

23. Gustavsson, S A L

Calculation of body interference loads for wing-body combinations at Mach numbers from 1.59 to 7.15 with supersonic linear theory.
FFA AU-635, Part 1, 1971.

24. Larson, E
Agrell, N

Wing-body interference at moderate supersonic speeds. A comparison between panel method and experiment.
FFA TN AU-940, 1975.

25. RAE, W J

Generalized distribution along the body axis of the increment in lift produced by interference from the wing.
Cornell Aeronautical Laboratory, Bumblebee Report CAL/CM-794.

26. Larson, E

Wing-body interference. On a generalized load distribution on the body due to triangular wings at supersonic speeds.
FFA TN AE-1253. 1976.